2025 IEEE 2nd International Conference on Information Technology, Electronics and Intelligent Communication Systems (ICITEICS)
Bengaluru, India. Aug 29-30, 2025

2025 IEEE 2nd International Conference on Information Technology, Electronics and Intelligent Communication Systems (ICITEICS) | 979-8-3315-0784-8/25/$31.00 ©2025 IEEE | DOI: 10.1109/ICITEICS64870.2025.11341149

Whale Optimization for Parameters Estimation of 4H-SiC MESFET Including Trappings and Thermal Effects

Gowtham Raj R
Assistant Professor, Mechanical Engineering Department, New Horizon College of Engineering,
Bengaluru, India, Email: gowthamiitdh19@gmail.com.

Mohammad Aasim Khan
Assistant Professor, Department of Mathematics & Statistics Integral University,
Lucknow, India, Email: khan.aasim012@gmail.com.

Abhishek Agarwal
Professor, Department of Mechanical Engineering, College of Science and Technology, Royal University of Bhutan,
Phuentsholing, Bhutan, Email: agarwala.cst@rub.edu.bt.

G. Divya
Assistant Professor, Department of Electrical and Electronics Engineering, CVR College of Engineering,
Hyderabad, Telangana, India, Email: divya.gongidi@gmail.com.

Upendra Aswal
Associate Professor, Department of Computer Science and Engineering, Graphic Era Deemed to Be University,
Dehradun, India, Email: aswal_upendra.cse@geu.ac.in.

R. Ahila
Professor, Department of CSE, New Prince Shri Bhavani College of Engineering and Technology,
Chennai, Tamil Nadu, India, Email: ahila.r@newprinceshribhavani.com.

N. Karuppiah
Professor, Department of EEE, Vardhaman College of Engineering,
Hyderabad, Telangana, India, Email: natarajankaruppiah@vardhaman.org.

Suresh Kakinatla*
Researcher, CPGC Pvt. Ltd and ERG Foundation, Anakapalli,
Visakhapatnam, Andhra Pradesh, India.
Email: suresh@erg.org.in.

***Abstract*: 4H-SiC MESFETs are used for many applications including home, industries, and many more. Many approaches are available to analyze the model of the 4H-SiC MESFETs. The examination of MESFETs in relation to their direct current characteristics is a complex endeavor. This paper focuses on three primary factors that influence these characteristics: surface trapping, thermal effects, and substrate trapping. By exploring these effects, we aim to provide a clearer understanding of the DC behavior of MESFETs. The model for the current-voltage (I-V) characteristics that we present is based on the Caughey-Thomas configuration. This model effectively addresses the trapping of electrons in the substrate through various deep-level trapping mechanisms, takes into account the field-dependent mobility of electrons, and provides a detailed analysis of the two-dimensional charge distribution that occurs beneath the gate of the MESFET. This proposed method is comprehensive, accounting for all significant thermal effects and material flaws, including traps. Despite the challenges posed by the complexity of intricate mathematical equations associated with the 4H-SiC MESFET, which are essential for deriving accurate I-V characteristics across different operational regions, a solution is sought. To tackle this issue, the Whale Optimization Algorithm (WOA) is utilized, enabling the effective resolution of multiple complex equations related to the 4H-SiC MESFET. This approach ensures that the resulting I-V characteristics are precise and reliable. As a result, the performance of the analytical model developed closely mirrors that of a real 4H-SiC MESFET. Additionally, various behavioral traits of the model are obtained and thoroughly evaluated using the MATLAB programming.**

Keywords—MESFET, Whale optimization, Self heating effects, 4H-SiC; Multiple Trapping; Thermal effects.

I. Introduction

Electronic semiconductor devices, such as Bipolar Junction Transistors (BJTs), Metal-Oxide-Semiconductor Field-Effect Transistors (MOSFETs), and Metal-Semiconductor Field-Effect Transistors (MESFETs), play a crucial role in a multitude of applications that we encounter daily [1-2]. These devices are integral to the functioning of various electronic systems and technologies, making them indispensable in modern society. Silicon Carbide (SiC) is recognized as a particularly important material for the development of high-power microwave circuits and radio frequency (RF) circuitry, due to its outstanding properties that enhance performance and efficiency [3-4]. Among the different types of MESFETs, certain characteristics distinguish them, rendering them particularly well-suited for a diverse range of applications and modules, thereby expanding their use in the electronics industry.

The benefits of this material can be mainly attributed to its advantageous characteristics [5]. These are include a wide bandgap that allows for efficient operation even in high voltage situations, a high saturated electron velocity that boosts the operational speed of electronic devices, a significant breakdown field that enables the material to endure high electric fields without failure, and exceptional thermal conductivity that supports effective heat dissipation during operation. SiC has a range of features that make it an excellent option for requiring strong performance in challenging environments. The unique material properties of 4H-SiC MESFETs will be employed to develop advanced microwave circuits, contingent upon the confirmation that the 4H-SiC substrate is semi-insulating (SI) [6].

The standard technique for creating SI substrates typically involves the addition of deep level dopants. These dopants are essential for ensuring that the Fermi level (FL) is situated at the midpoint of the bandgap, a condition that is crucial for achieving the desired electrical properties. Nevertheless, the presence of material defects significantly complicates the production of high purity semi-insulating (HPSI) substrates. Although HPSI substrates can be manufactured, this process often results in the introduction of extra deep levels within the material. These deep levels can act as traps for charge carriers, leading to a reduction in the performance of electronic devices that are constructed on these substrates.

The effects of substrate and surface trapping phenomena play a critical role in determining device performance, particularly through issues like current collapse in direct current characteristics, variations in transconductance that depend on frequency, and the lag transients linked to both drain and gate operations [7-8]. These elements collectively reduce the overall power efficiency of the device. Thus, it is essential to develop accurate models that consider these trapping effects to facilitate a precise evaluation of SiC devices. This modeling is crucial for understanding the impact of these phenomena on device behavior and for enhancing their performance in practical applications. Therefore, the paper should incorporate a detailed modeling approach to achieve characteristics that closely resemble those of a real-time MESFET.

The MESFET model is characterized by a set of nonlinear equations that present significant challenges in terms of solving them directly, often requiring specific assumptions to simplify the process. At the same time, a range of optimization methods is utilized to effectively manage various nonlinear and intricate functions. Notably, the Whale Optimization Algorithm (WOA) has emerged as a particularly effective optimization technique [9-10], recognized for its strength in addressing complex nonlinear mathematical functions.

Recent studies conducted by various researchers have yielded significant insights, which are summarized in the following paragraph. The authors cited in reference [11] perform a power density analysis of the 4H-SiC MESFET. In reference [12], the focus is on the displacement damage related to the 4H-SiC MESFET. A simulation study regarding the 4H-SiC MESFET has been executed by the authors in reference [13]. The power characteristics of the dual-channel 4H-SiC MESFET are detailed by the authors in reference [14]. Reference [15] addresses the simulation and design considerations relevant to the 4H-SiC MESFET. The fabrication aspects of the 4H-SiC MESFET are outlined by the authors in reference [16]. A comparative analysis of various 4H-SiC MESFETs is conducted by the authors in reference [17]. The authors in reference [18] present an analysis of low insulator fields in 4H-SiC. The integration of a bulgy channel to enhance MESFET performance is discussed by the authors in reference [19]. The performance of the 4H-SiC MESFET across lightly doped, heavily doped, and insulated regions is investigated by the authors in reference [20]. Enhanced characteristics of the 4H-SiC MESFET are achieved through the integration of a partially undoped and low-doped region, as elaborated in references [21-22]. This paper offers a comprehensive analytical framework for the direct current operation of 4H-SiC MESFETs, taking into account all critical trapping effects and thermal influences that significantly affect the performance of these devices.

The remainder of the manuscript is structured by offering an in-depth analysis of the model in Section II. The methodology of the WOA approach for addressing complex functions is detailed in Section III. A variety of results and analyses are showcased in Section IV. Conclusions are formulated in Section V. Important references are compiled in the references section.

II. Analysis

This document presents a comprehensive proposed model that details the direct current characteristics of 4H-SiC MESFETs. It takes into account all relevant trapping phenomena and thermal effects that could influence the performance of the device. The model includes the bias dependence of the series resistances at both the source (R_S) and drain (R_D) terminals, which are critical for understanding the device's behavior under different operating conditions. Figure 1 provides a detailed schematic cross-section of the MESFET, highlighting its structural components and overall layout, which are essential for grasping the device's design and functionality. In contrast, Figure 2 focuses on the depletion regions located on the surface of the device in the ungated areas. This figure offers valuable insights into the electrical characteristics and behavior of these regions, which are important for understanding the device's performance.

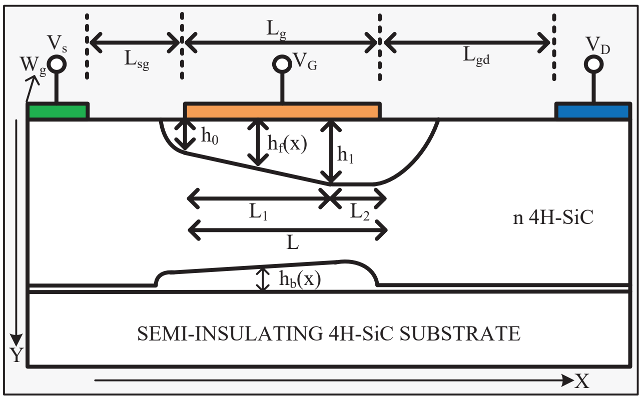

Fig. 1: Schematic structure with back depletion region of 4H-SiC MESFET.

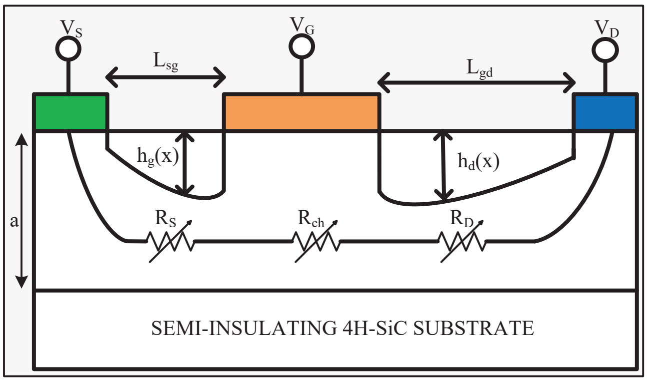

Fig. 2: Schematic structure with depletion region at ungated portions.

This trapping phenomenon pertains to the influence of three primary deep level traps, namely $Z_{1/2}$, $EH_{6/7}$, and $RD_{1/2}$, which have been recognized in the HPSI substrate of 4H-SiC. These traps significantly contribute to the reduction of channel current, as demonstrated in the I-V characteristics of the material. When these traps capture charge carriers, they obstruct the current flow, resulting in a marked decrease in the overall channel current observed during electrical measurements. The various types of deep level traps (DLT) found in the material are categorized as acceptor types. The position of the FL within the substrate's bulk will be established by implementing the neutrality charge conditions.

$$n + N_{SA}^{-} + N_{sub}^{-} = p + N_{SD}^{+} \qquad (1)$$

here $N_{SD}^{+}, n, p,$ and N_{SA}^{-} denotes the ionized shallow donor, free electrons, holes, and acceptor concentration, N_T^{-} is the density of ionized traps in the bulk substrate.

The overall concentration of negative charge is primarily indicated on the substrate side, especially in proximity to the interface of the channel substrate (CS). This concentration is influenced by the occupancy probability of deep traps that are situated within the bulk material. The connection between these factors can be expressed mathematically through the following equation:

$$N_{sub}^{-} = \left(\sum_{i=1}^{3} f_{T(non-eql)} - \sum_{i=1}^{3} f_{T(eql)} \right) N_T^{-} \tag{2}$$

$$N_{sub}^{-} = \sum_{i=1}^{3} N_T^{-} \left(\frac{e_{pT}}{e_{pT} + e_{nT}} \right) - \sum_{i=1}^{3} N_T^{-} \left(1 + \frac{1}{g} e^{\frac{\left(E_T - E_f\right)}{KT}} \right) \tag{3}$$

here $e_{pT}\left(e_{nT}\right)$ represents the rate of the emission of holes, E_T & E_f are the trap and FL energies respectively.

A surface trapping phenomenon denotes a decrease in current resulting from the presence of trapped charges within the channel. These charges are located in the ungated regions situated between the gate and source points, as well as in the areas between the drain and gate points. The effect of series resistance at the drain point (R_D) and source series resistance (R_S) illustrated in Figure 1 (b) is projected where the R_S or R_D values are resistances and are state density of non-uniform interfaces $\left(D_{it}\right)$. This D_{it} profile is segregated as three sections [3-6] i.e., conduction band edge $\left(D_{it}^{CBedge}\right)$, and distribution of D_{it} valences band edge $\left(D_{it}^{VBedge}\right)$, and at the middle $\left(D_{it}^{mid}\right)$. D_{it} is mathematical expression is represented by below equation.

$$D_{it}(E) = D_{it}^{mid} + D_{it}^{CBedge} e^{\left(\frac{E - E_{fs}}{\sigma(t)}\right)} + D_{it}^{VBedge} e^{\left(\frac{E_{fs} - E}{\sigma(t)}\right)} \tag{4}$$

where E_{fs} is the surface FL.

Taking into account the irregular distribution of D_{it}, the voltage at surface built-in ϕ_{sbi} is defined as an expression of D_{it} and is utilized in the computation of ungated R_S at section. The expression below is employed to calculate the potential at surface built-in section.

$$W_D = \frac{1}{N_d} \int_{E_0}^{E_{fs}} D_{it}(E) f(E) dE \tag{5}$$

where W_D is the region at surface depletion width at the surface source side, doping concentration represented by N_d, and $f(E)$ represents the function of Fermi distribution.

$$W_D = \left(\frac{2\varepsilon\phi_{sbi}}{qN_d} \right)^{1/2}, \quad f(E) = \frac{1}{1 + \frac{e^{\left(\frac{E_T - Efs}{KT}\right)}}{g}}$$

The updated model illustrates the influence of R_S and R_D on the I-V properties under various surface scenarios (D_{it} profile). Figure 3 illustrates the relationship between R_S and R_D as they vary with the gate bias.

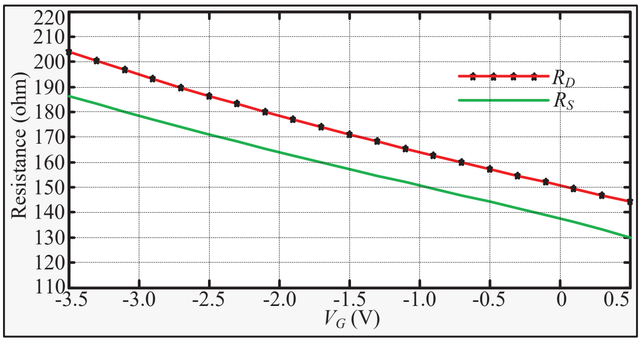

Fig. 3: Plot of R_D and R_S versus V_G.

The self-heating phenomenon refers to a complex interplay of factors including low field mobility, the impact of temperature on velocity saturation, and the levels of free carrier concentrations within a semiconductor device. When the drain voltage is increased, there is a corresponding decrease in the drain current observed. To accurately determine the I-V characteristics of the device, an iterative method is employed. This method involves systematically adjusting the temperature and drain voltages to observe how these changes affect the current flow, as documented in reference [7]. Other parameters are obtained from [23-32].

The MESFET model utilized to illustrate the I-V characteristics employs the Caughey-Thomas representation, which effectively illustrates the impact of the electric field on electron mobility. This model also accounts for the phenomenon of substrate trapping, wherein electrons are captured by various deep-level traps typically present in 4H-SiC materials. Additionally, the model offers a comprehensive analysis of the charge distribution occurring in two dimensions beneath the gate, thus providing valuable insights into the device's performance under varying operating conditions. The instantaneous current within the channel, taking into account the mobility that is field-dependent, is expressed as:

$$I_D = q\mu(E)E(x)Wn(x)[a - h(x)] \tag{6}$$

here a represents epitaxial layer thickness, Width is W, $\mu(E)$ represents field dependent mobility, thickness of the depletion layer is $h(x)$, and $n(x)$ represents concentration of the electrons.

The modified properties of a MESFET that includes surface and substrate trappings can be represented as [7]:

$$I_D = YaV_P \left[\left[\left(\frac{V_D - I_D(R_S + R_D)}{V_P} \right)^{1/2} - \frac{2}{3}\left(U_D^3 - U_S^3\right) - \frac{2}{3} k_{11} \left(U_{1D}^3 - U_{1S}^3\right) \right] \right] \tag{7}$$

here, drain bias represented by V_D , V_p and k_{11} are constants

$$V_P = \frac{qN_d a^2}{2\varepsilon_s}, \quad k_{11} = \left(\frac{N_{sub}^-}{N_{sub}^- + N_{dep}^+}\right)^{1/2}$$

$$Y = \frac{qWv_{sat}\mu_0\left(N_d - N_{sub}^-\right)}{v_{sat}L + \mu_0\left[V_D - I_D\left(R_S + R_D\right)\right]}$$

$$U_D = \left(\frac{V_{bi} - V_G + V_D - I_D R_D}{V_P}\right)^{1/2}, \quad U_{1S} = \left(\frac{U_{bi} + I_D R_S}{V_P}\right)^{1/2}$$

$$U_S = \left(\frac{V_{bi} - V_G + I_D R_S}{V_P}\right)^{1/2} \quad U_{1D} = \left(\frac{U_{bi} + V_D - I_D R_D}{V_P}\right)^{1/2}$$

,

Width of the normalized depletion of the channel is $U_{1D}(U_{1S})$, and $U_D(U_S)$ represents the width of the normalized depletion of gate drain(source). V_G is the negative gate bias v_{sat} is the saturation velocity, and V_{bi} indicates the schottky gate built in potential value.

By integrating modulation length of the channel, the channel beneath the gate is segmented into a pinch-off ($L - L_1$) and linear regions (L_1), as illustrated in Figure 1. Then:

$$I_D = Y_1 a V_P \left[\left(\frac{V(L_1) - I_D R_S}{V_P}\right) - \frac{2}{3}\left(U_{L1}^3 - U_S^3\right) - \frac{2}{3}k_{11}\left(U_{1L1}^3 - U_{1S}^3\right)\right] \quad (8)$$

where

$$Y_1 = \frac{qWv_{sat}\mu_0\left(N_d - N_{sub}^-\right)}{v_{sat}L_1 + \mu_0\left(V(L_1) - I_D R_S\right)},$$

$$U_{L1} = \left(\frac{V_{bi} - V_G + V(L_1)}{V_P}\right)^{1/2} \quad U_{1L1} = \left(\frac{U_{bi} + V(L_1)}{V_P}\right)^{1/2}$$

U_{L1} is the width of the normalized depletion and U_{1L1} is the depletion width at interface of CS.

A two-dimensional examination of equations for determining the potential within the depletion portion beneath the gate is articulated as:

$$V_D - R_D I_D = V(L_1) + \frac{2E_c a\left(\frac{V_{bi} - V_G + V(L_1)}{V_P}\right)^{1/2}}{\pi} \sinh\left(\frac{\pi(L - L_1)}{2a\left(\frac{V_{bi} - V_G + V(L_1)}{V_P}\right)^{1/2}}\right) \quad (9)$$

The existing expression above in the region under saturation beyond $x = L_1$ is

$$I_D = \gamma a W q\left(N_d - N_{sub}^-\right)v_{sat}\left(1 - U_{1L1}k_{11} - U_{L1}\right) \quad (10)$$

III. WOA Approach For Nonlinear I-V Functions

The Whale Optimization Algorithm (WOA) [9-10] is a sophisticated metaheuristic optimization technique that takes its inspiration from the unique hunting behaviors of humpback whales. This algorithm mimics various strategies that these whales use in their natural habitat, such as encircling their prey, executing bubble-net feeding techniques, and systematically searching for food sources. By emulating these behaviors, WOA aims to identify optimal solutions to complex problems. It is widely recognized as a highly effective optimization method and is frequently utilized in a variety of fields, including computer science, engineering, and other areas that require efficient problem-solving techniques. The hunting technique of Whales is graphically represented in Figure 4.

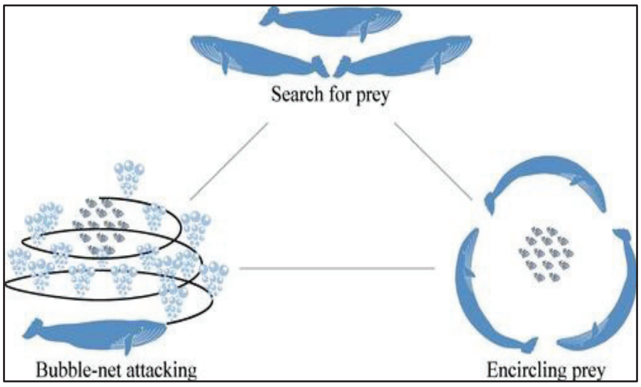

Fig. 4: Hunting behavior of Whales.

Humpback whales are renowned for their distinctive hunting techniques, especially in relation to the WOA. These extraordinary animals demonstrate an impressive capability to surround their prey by swimming in increasingly tighter circles, all while following a spiral trajectory. This elaborate hunting strategy not only reflects their cognitive abilities but also emphasizes the intricate relationships within marine ecosystems. The mathematical models that depict this hunting behavior and the related actions of humpback whales are crucial and can be represented through various equations and diagrams that illustrate the dynamics of their movements and tactics. The WOA method serves as a highly effective tool for solving numerous complex equations in a very short time frame. Therefore, the various intricate mathematical equations discussed in this paper are efficiently resolved using the WOA technique. Below mathematical expressions are involved in the process of the WOA.

$$\vec{H} = \left|\vec{V}(\mathrm{t}) - \vec{C} \bullet \vec{V}^*(\mathrm{t})\right| \quad (16)$$

$$\vec{V}(\mathrm{t}+1) = \vec{V}^*(\mathrm{t}) - \vec{\mathrm{A}} \bullet \vec{H} \quad (17)$$

$$\vec{H}' = \vec{V}^*(\mathrm{t}) - \vec{V}(\mathrm{t}) \quad (18)$$

$$\vec{V}(\mathrm{t}+1) = \begin{cases} \vec{V}^*(\mathrm{t}) - \vec{\mathrm{A}} \bullet \vec{H} & \text{if } q < 0.5 \\ \vec{H}' \bullet \mathrm{e}^{\mathrm{bl}} \bullet \cos(2\pi l) + \vec{V}^*(\mathrm{t}) & \text{if } q \geq 0.5 \end{cases} \quad (19)$$

$$\vec{H} = \left|\vec{C} \bullet \vec{V}_{rand} - \vec{V}\right| \quad (20)$$

$$\vec{V}(\mathrm{t}+1) = \vec{V}_{\mathrm{rand}} - \vec{\mathrm{A}} \bullet \vec{H} \quad (21)$$

$$\vec{A} = 2\vec{a} \bullet \vec{r} - \vec{a} \quad (22)$$

$$\vec{C} = 2 \bullet \vec{r} \quad (23)$$

$$\vec{V}(\mathrm{t}+1) = \vec{V}^*(\mathrm{t}) + \vec{H}' \bullet \mathrm{e}^{\mathrm{bl}} \bullet \cos(2\pi l) \quad (24)$$

Where, coefficient vectors are $\vec{A}$ and $\vec{C}$, 't' is iteration, $\vec{V}^*$ and $\vec{V}$ are position vectors of best and present solutions.

The optimal voltage and current points for a 4H-MESFET, at which it can generate best curve suitated to experimental shape, is referred to as the best solution. In every iteration, the locations of the participants are modified, and the targeted mathematical expression is assessed. The optimal value of the best solution will be considered as the identifier for the 4H-SiC MESFET characterization equation.

IV. Analysis and Results

This section presents a range of results obtained from the MATLAB programming environment. To begin with, we assess the performance of the WOA in comparison to other well-established optimization methods, including Particle Swarm Optimization (PSO) and Ant Colony Optimization (ACO). The convergence rates associated with solving the intricate equation of the 4H-SiC MESFET, along with its performance capabilities, are depicted in Figure 5. This figure clearly illustrates that the proposed WOA significantly surpasses the performance of the existing PSO and ACO techniques. As a result, we have also gathered additional findings utilizing the WOA method. Computational complexity, convergence time and robustness are the main parameters to choose the optimization method. Comparisons among PSO, ACO and proposed WOA on these parameters are presented in Figure 6. From Figure 6, the proposed WOA method is better than PSO and ACO methods.

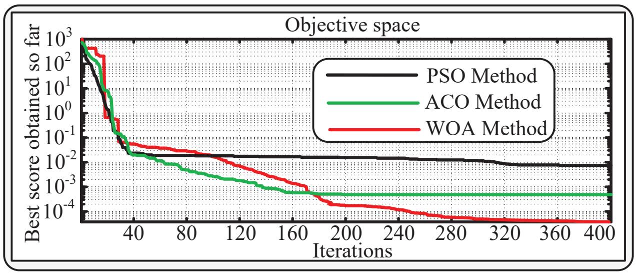

Fig. 5: Performance comparison among PSO, ACO and WOA.

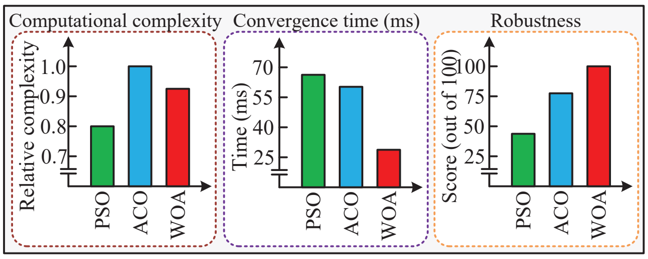

Fig. 6: Various responses of proposed WOA over PSO and ACO.

Figure 7 and 8 present the direct current characteristics of the MESFET, which have been derived from the previously mentioned data using mathematical equations. The results depicted, especially in Figure 7, demonstrate a significant correlation with the experimental validations referenced in [7]. Furthermore, a comparison is drawn between the current models that incorporate self-heating effects and those that do not include such features. In addition, Figure 8 provides a more detailed comparison between the models with self-heating and those without, specifically in relation to current behavior.

The unpassivated surface, combined with the distances from the source to the gate and from the gate to the drain, results in a high density of D_{it} , which contributes to surface trapping. The overlap of the depletion region between the gate and source, as well as between the gate and drain, leads to a rise in R_S & R_D . As a result, the current failure becomes apparent in the I-V curves. The dependence of R_S & R_D on bias adds further complexity to the model; nevertheless, it may produce characteristics that more accurately reflect those of the real 4H-SiC MESFET.

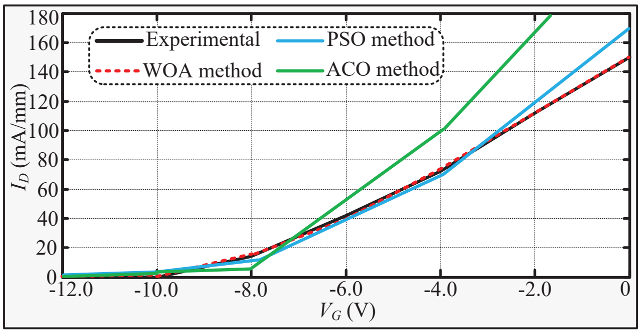

Fig. 7: I_D-V_G properties with surface and substrate trappings.

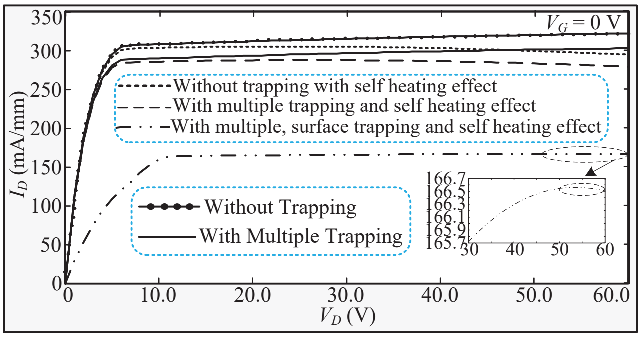

Fig. 8: I_D-V_D curves with effects of self heating.

Figure 9 presents a comparative analysis of the 4H-SiC MESFET, showcasing the results obtained with the WOA, without WOA, and from experimental curves across various gate voltages.

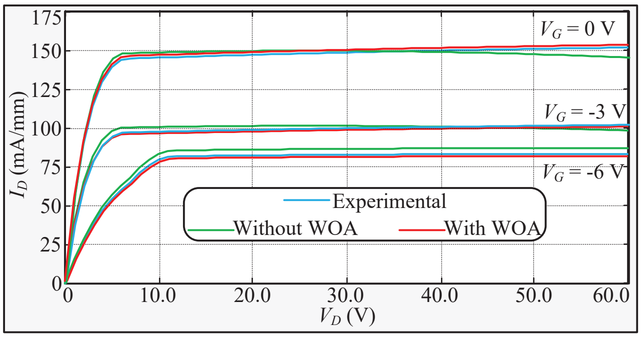

Fig. 8: Responses with and without WOA.

The data derived using WOA, which involves solutions from a range of mathematical equations, shows a strong correlation with the experimental curves. This is particularly evident when compared to the results from traditional mathematical methods that do not utilize WOA. The effectiveness of WOA can be attributed to its ability to deliver rapid and accurate solutions for the intricate nonlinear mathematical equations that describe the behavior of 4H-SiC MESFET. The methodology proposed in this analysis successfully captures the I-V characteristics of the MESFET with high accuracy and reliability. Consequently, this approach is considered more suitable for guiding future research in this area.

V. Conclusion

We introduce a sophisticated proposed model that precisely characterizes the direct current properties of 4H-SiC MESFETs. This model comprehensively accounts for all varieties of material defects by employing a WOA technique. As a result, it facilitates an in-depth examination of the device's performance across a range of operational conditions. Furthermore, we provide an extensive comparison of the current behavior between models that include charge trapping effects and those that exclude them, emphasizing the notable discrepancies in their predictive outcomes. The impact of bias dependence and the density of interface states of R_S (R_D) is also considered. The results based on simulations are obtained demonstrate a closer correlation with the experimental $I_D - V_G$ curves. The proposed analysis has the potential to significantly enhance our comprehension of MESFET behavior at microwave frequencies. It has been observed that the WOA-based method put forward exhibits accurate and consistent characteristics when applied to the 4H-SiC MESFET, making it a valuable tool for researchers in this field.

References

[1]. D. Kim et al., "Static, Dynamic, and Short-circuit Characteristics of Split-Gate 1.2 kV 4H-SiC MOSFETs," 2023 IEEE International Reliability Physics Symposium (IRPS), Monterey, CA, USA, 2023, pp. 1-4, doi: 10.1109/IRPS48203.2023.10118091.

[2]. H. A. Moghadam, S. Dimitrijev, J. Han, D. Haasmann and A. Aminbeidokhti, "Transient-Current Method for Measurement of Active Near-Interface Oxide Traps in 4H-SiC MOS Capacitors and MOSFETs," in IEEE Transactions on Electron Devices, vol. 62, no. 8, pp. 2670-2674, Aug. 2015, doi: 10.1109/TED.2015.2440444.

[3]. V. Van Cuong, T. Meguro, S. Ishikawa, T. Maeda, H. Sezaki and S. -I. Kuroki, "Thermal Stability of Gate Driver Circuits Based on 4H-SiC MOSFETs at 300°C for High-Power Applications," in IEEE Journal of the Electron Devices Society, vol. 13, pp. 161-167, 2025, doi: 10.1109/JEDS.2025.3546959.

[4]. A. Shimbori and A. Q. Huang, "A Novel 600V Lateral RESURF 4H-SiC MESFET with Sloped Field Plate for High Power and High Frequency Applications," 2020 IEEE Workshop on Wide Bandgap Power Devices and Applications in Asia (WiPDA Asia), Suita, Japan, 2020, pp. 1-5, doi: 10.1109/WiPDAAsia49671.2020.9360295.

[5]. Roustaie, Z., Orouji, A.A. Novel 4H-SiC MESFET with amended minimum noise figure for high-frequency applications. *J Comput Electron* **24**, 81 (2025). https://doi.org/10.1007/s10825-025-02322-5.

[6]. V. Banu, P. Godignon, M. Alexandru, M. Vellvehi, X. Jordà and J. Millán, "Demonstration of temperature compensated voltage reference integrated circuit designed with 4H-SiC MESFETs," 2014 International Semiconductor Conference (CAS), Sinaia, Romania, 2014, pp. 233-236, doi: 10.1109/SMICND.2014.6966445.

[7]. V. Banu, P. Godignon and J. Millán, "Design of voltage comparator integrated circuit with normally-on MESFETs on 4H-SiC semiconductor," 2015 International Semiconductor Conference (CAS), Sinaia, Romania, 2015, doi: 10.1109/SMICND.2015.7355198.

[8]. Hu-jun Jia, Zhi-hui Yang, Pei-miao Ma, Qiu-yuan Wu and Ye-hui Luo, "A novel 4H-SiC MESFET with localized high-doped P-buffer layer," 2016 13th IEEE International Conference on Solid-State and Integrated Circuit Technology (ICSICT), Hangzhou, China, 2016, pp. 1086-1088, doi: 10.1109/ICSICT.2016.7998658.

[9]. N. Katta, et al., "Whale Optimization based MPPT of Single Stage Grid Connected PV System with H∞ Controller", 2022 *1st IEEE International Conference on Industrial Electronics: Developments & Applications (ICIDeA)*, Bhubaneswar, India, 2022, pp. 220-226, doi: 10.1109/ICIDeA53933.2022.9970020.

[10]. S. G. Malla et al., "Whale Optimization Algorithm for PV Based Water Pumping System Driven by BLDC Motor Using Sliding Mode Controller", *IEEE Journal of Emerging and Selected Topics in Power Electronics*, Vol. 10, No. 4, pp. 4832-4844, Aug. 2022, doi: 10.1109/JESTPE.2022.3150008.

[11]. X. Zhang and N. You, "Power density of the optimized dual-channel 4H-SiC MESFETs," 2017 Chinese Automation Congress (CAC), Jinan, China, 2017, pp. 1261-1264, doi: 10.1109/CAC.2017.8242960.

[12]. S. C. Witczak, W. A. Martin, J. W. Palko, J. R. Srour and R. Koga, "Displacement Damage in an Irradiated 4H-SiC MESFET," in IEEE Transactions on Nuclear Science, vol. 72, no. 5, pp. 1755-1762, May 2025, doi: 10.1109/TNS.2025.3550298.

[13]. X. Zhang and M. Wang, "Simulation of high power step-buffer 4H silicon carbide metal semiconductor field effect transistor," 2018 International Conference on Electronics Technology (ICET), Chengdu, China, 2018, pp. 1-5, doi: 10.1109/ELTECH.2018.8401426.

[14]. X. Zhang and N. You, "Power Characteristics for the Dual Channel 4H-SiC Metal Semiconductor Field Effect Transistor," 2018 IEEE 3rd International Conference on Integrated Circuits and Microsystems (ICICM), Shanghai, China, 2018, doi: 10.1109/ICAM.2018.8596550.

[15]. Y. Bai, et. al., "Design and simulation of 4H-SiC MESFET ultraviolet photodetector with gain," 2016 European Conference on Silicon Carbide & Related Materials (ECSCRM), Halkidiki, Greece, 2016, pp. 1-1, doi: 10.4028/www.scientific.net/MSF.897.610.

[16]. A. Shimbori and A. Q. Huang, "Design and fabrication of low pinch-off voltage 700V lateral 4H-SiC MESFET with thin RESURF layer," 2021 Device Research Conference (DRC), Santa Barbara, CA, USA, 2021, pp. 1-2, doi: 10.1109/DRC52342.2021.9467247.

[17]. D. A. Prasad and R. Komaragiri, "Performance comparison of 4H-SiC mesfets," Annual International Conference on Emerging Research Areas and 2013 International Conference on Microelectronics, Communications and Renewable Energy, Kanjirapally, India, 2013, doi: 10.1109/AICERA-ICMiCR.2013.6575965.

[18]. P. Fiorenza et al., "Consideration on the extrapolation of the low insulator field TDDB in 4H-SiC power MOSFETs," 2023 IEEE International Reliability Physics Symposium (IRPS), Monterey, CA, USA, 2023, pp. 1-4, doi: 10.1109/IRPS48203.2023.10118116.

[19]. Hujun Jia, Yunfan Zhang, Huan Wang, Shunwei Zhu, Xiaojie Wang, Yangyi Shen, Yintang Yang, Improved 4H–SiC MESFET with bulgy channel, Micro and Nanostructures, Volume 166, 2022, https://doi.org/10.1016/j.micrna.2022.207222.

[20]. Jia, H.; et. al.,. A Novel 4H-SiC MESFET with a Heavily Doped Region, a Lightly Doped Region an Insulated Region, *Micromachines* **2021**, *12*, 488. https://doi.org/10.3390/mi12050488.

[21]. Jia, H., Wang, X., Shen, Y. *et al.* Improved 4H-SiC MESFET with Partially Undoped Region and Tortuous Channel. *Silicon* **15**, 7725–7732 (2023). https://doi.org/10.1007/s12633-023-02623-z.

[22]. Jia, H.; et. al.; Yang, Y. An Improved 4H-SiC MESFET with a Partially Low Doped Channel. *Micromachines* **2019**, Vol. *10*, 555. https://doi.org/10.3390/mi10090555.

[23]. Alluri Navaneetha; Dumpa Prasad; S. Aruna Deepthi; A. Kishore Reddy; Adama Jashwanth Chandhra; Asisa Kumar Panigrahy, "Analysis of nanowire FET over FinFET", AIP Conference proceedings, Vol. 2492, May 2023, https://doi.org/10.1063/5.0114054.

[24]. Kuppahalli P., Keshavamurthy R., Sriram P., Narayana A. (2021). The influence of silicon addition on microstructure and mechanical properties of manganese bronze alloys. *Iranian Journal of Materials Science and Engineering*, 18(2). https://doi.org/10.22068/ijmse.2063.

[25]. Sateesh Kumar Palla, "A Review on Power Electronic Switching Devices and its Applications", International Journal of New Technologies in Science and Engineering (IJNTSE), Vol. 11, Issue. 1, pp. 1-8, Jan. 2025.

[26]. Dravid S, Chinchanikar S, Ambhore N, Gadage M, Somatkar A, et al. 2024. Investigation on Varying Weight Percentage of Nickel Nanoparticles on the Thermal Properties of Polymeric Nanocomposites. NanoWorld J 10(S1): S488-S493.

[27]. Kumar S, Sharma SS, Giri J, Makki E, Sathish T and Panchal H (2024) Perovskite materials with improved stability and environmental friendliness for photovoltaics. Front. Mech. Eng 10:1357087. doi: 10.3389/fmech.2024.1357087.

[28]. Thirunavukkarasu Mylswamy et. al., "Feature of SiO2 concentration on solar thermal functional characteristics of flat plate solar collector", Thermal Science 2024 Volume 28, Issue 1 Part A, Pages: 249-255, https://doi.org/10.2298/TSCI230417275T.

[29]. M. G. Al-Ghanimi et al., "Two TS-Fuzzy Controllers based Direct Torque Control of 5-Phase Induction Motor", *2022 IEEE International Conference on Power Electronics, Drives and Energy*

Systems (PEDES), Jaipur, India, 2022, pp. 1-6, doi: 10.1109/PEDES56012.2022.10080625.

[30]. P. Pal, R. K. Behera and U. R. Muduli, "Feedforward Repetitive Approach to Disturbance Rejection in DAB Converters for EV Charging," *IEEE Transactions on Industrial Electronics*, doi: 10.1109/TIE.2024.3519565.

[31]. Krishnappa, K. H., Hiremath, M. M. ., R., M. ., R., M. ., Holla K., N. ., & Gomathi, P. (2023). Semiconductor Fault Diagnosis Using Deep Learning-Based Domain Adaption. International Journal of Intelligent Systems and Applications in Engineering, 12(9s), 391–404.

[32]. P. Pal, R. K. Behera and U. R. Muduli, "Feedforward Repetitive Approach to Disturbance Rejection in DAB Converters for EV Charging," *IEEE Transactions on Industrial Electronics*, doi: 10.1109/TIE.2024.3519565.